The kidnapping of mitochondrial function associated to the SARS-CoV-2 infection

Elizabeth Soria-Castro
Instituto Nacional de Cardiología Ignacio Chávez
María Elena Soto
Instituto Nacional de Cardiología Ignacio Chávez
Verónica
Guarner-Lans
Gustavo Rojas
Instituto Nacional de Cardiología Ignacio Chávez
Mario Perezpeña-Diazconti
Instituto Nacional de Cardiología Ignacio Chávez
Sergio A Críales-Vera
Instituto Nacional de Cardiología Ignacio Chávez
Linaloe Manzano Pech
Instituto Nacional de Cardiología Ignacio Chávez
Israel Pérez-Torres (pertorisr@yahoo.com.mx)
Instituto Nacional de Cardiología Ignacio Chávez

Research Article

Keywords: SARS-CoV-2, mitochondria, electron transport chain, COVID-9, nitrosative stress

Posted Date: December 31st, 2020

DOI: https://doi.org/10.21203/rs.3.rs-137853/v1

Version of Record: A version of this preprint was published on June 16th, 2021. See the published version at https://doi.org/10.14670/HH-18-354.

Abstract

Severe Acute Respiratory Syndrome Coronavirus 2 (SARS-CoV-2) infection leads to multiorganic failure associated with a cytokine storm and septic shock. The virus evades the mitochondrial production of interferons through its N protein. From that moment on, SARS-CoV-2 hijacks the functions of this organelle. The aim of this study was to show how the virus kidnaps the mitochondrial machinery for its benefit and survival, altering serum parameters and leading to nitrosative stress (NSS). In a prospective cohort of 15 postmortem patients who died from COVID-19, six markers of mitochondrial function; COX II, COX IV, MnSOD, nitrotyrosine, Bcl-2 and caspase-9 were analyzed by the immune colloidal gold technique in samples from the lung, heart, kidney and liver. Biometric laboratory results from these patients showed alterations in hemoglobin, platelets, creatinine, urea nitrogen, glucose, C-reactive protein, albumin, D-dimer, ferritin, fibrinogen, Ca^{2+}, K^{+}, lactate and troponin. These changes were associated with alterations of the mitochondrial structure and function. The multiorganic dysfunction present in COVID-19 patients may be caused in part by damage to the mitochondria that results in an inflammatory state that contributes to the elevation of NSS. NSS activates the sepsis cascade and contributes to the increased mortality in COVID-19 patients.

Introduction

By the end of December 2019, an outbreak of a new infection caused by the Severe Acute Respiratory Syndrome Coronavirus 2 (SARS-CoV-2) was reported (Singhal, 2020). When a viral infection occurs, an antiviral mitochondrial response is elicited to protect these organelles from the disruption caused by the virus. Mitochondria need to be protected from viral infections since they are indispensable, performing most of the catabolic processes required to produce ATP in the host, through activation of the electron transport chain (ETC) (Pérez-Torres et al., 2020). The different enzymes that participate in these processes and those of the citric acid cycle are found in the mitochondrial matrix. Mitochondria also need to be protected from the viruses since they play a critical role in antioxidant defenses containing catalase, super oxide dismutase (SOD) isoforms, thioredoxin 2, glutathione peroxidase 1 and 4, glutathione and α-keto acids which are also localized in the matrix. These enzymes detoxify the O_2^{-}, H_2O_2 and other free radicals generated both in the cytoplasm and in the mitochondria (Pérez-Torres et al., 2020). Furthermore, mitochondria also participate in the intermediary metabolism including that of pyrimidine, glutamine, urea, ammonia, and steroids (Mailloux, 2018). When mitochondrial functions are disrupted by a viral infection and the antiviral mitochondrial response is not able to counteract the infection, there is rupture of these organelles, and many of the enzymes they contain end up in the cytoplasm (Mailloux, 2018).

The antiviral mitochondrial response in initiated by the mitochondrial antiviral-signaling (MAVS) protein, which is an adaptor molecule of the retinoic acid-inducible gene I RIG-I and is localized in the mitochondrial outer membrane. This molecule directly binds with the viral RNA and transmits signals to induce the production of interferons (IFNs) (Hee and Cresswell, 2017). The IFNs system is the first line of defense of the host against viral invasions (Koshiba et al., 2011). The degradation of MAVS can inhibit the production of ATP by the mitochondria blocking the energy provision to the host, thus decreasing the antiviral system, and enhancing viral infection (Paumard et al., 2002). However, several viruses may also evade the antiviral mitochondrial response by damaging the mitochondrial DNA (Yin et al., 2017).

COVID-19 is also associated to a pro-inflammatory cytokine storm. The cytokine storm can block mitochondrial oxidative phosphorylation and it is associated with a low production of ATP (Paumard et al., 2002). Although this cytokine storm is the host's response to eliminate the virus, it is counterproductive for the host and can result in multi-organ failure (Soto et al., 2020). Some of the structural and non-structural proteins that are encoded by the RNA genome of SARS-CoV-2 may interact with mitochondrial components. Localization of the viral proteins in mitochondria is part of the strategy for kidnapping the host machinery and it is a necessary pathway for the establishment of the infection (Jean-Beltran et al., 2017).

Although few studies and computational models of SARS-CoV-2 viral RNA localization in the subcellular neighborhoods of the host, have suggested that the mitochondria are one of the main targets of SARS-CoV-2 (Jonathan et al., 2020; Wu et al., 2020), there is still no physical evidence of this fact. Therefore, the aim of this study was to show how SARS-CoV-2 may kidnap the mitochondrial machinery for its benefit without contemplating the repercussions that this entails for the host cells.

Materials And Methods

Ethics statement

This study was conducted in accordance with the principles of the declaration of Helsinki. This was an observational, comparative and descriptive study that was performed in a prospective cohort of 15 postmortem patients of COVID-19 that attended the Instituto Nacional de Cardiología “Ignacio Chávez”. All the procedures of this project which is in human participants of the National Institute of Cardiology Ignacio Chavez were within the ethical standards of the Institutional Research Committee and adhered to the agreements of the Declaration of Helsinki of 1964 with comparable ethical standards. The protocol was approved by the Research and Ethics Committee of our institution (Institutional protocol number: 20-1157). In this study, informed consent was obtained for medical care. In the cases, as patients who died, an informed consent was requested signed by the relatives for the postmortem study. Through an informed consent for the publication of the data was obtained from participants /legal guardian(s)/legally authorized representative/next of kin (for dead patients). That is, for to obtain the tissue by ultrasound-guided minimally invasive autopsy through the biopsy of the specific organ and with precautionary measures for the protection of the personnel of health that performed the biopsies.

Laboratory tests

The laboratory test were made in patients with COVID-19 to determine acute-phase reactants: Hemoglobin, leukocytes, lymphocytes, platelets, glutamic oxaloacetic transaminase (GOT), glutamic pyruvic transaminase (GPT), creatinine, urea nitrogen, glucose, C-reactive protein (CRP), albumin, D-dimer, ferritin, fibrinogen, Ca^{2+}, Cl^{-}, Na^{+}, K^{+}, pro-B-type natriuretic peptide (proBNP), lactate, troponin, and saturation oxygen. Data from the patient’s medical history including demographic data, schooling, type of occupation, habits, illnesses prior to infection by SARS-CoV-2, test result for COVID-19, whether mechanical ventilation was used and type of treatment given were used for the analysis of the results.

Control subject

The histological results of the patients with COVID-19 were compared with a control subject, which was 60-year-old female patient, negative for SARS-CoV-2. However, if presented hepatocarcinoma, pulmonary micro-metastases and symptoms of pulmonary hypertension. In this patient, there was no presence of degenerative disorders such as thyroid diseases, autoimmune diseases, and type 2 diabetes mellitus.

Obtainment of the post-mortem biopsies

Standard protective equipment was used to manage positive COVID-19 patients, including N95 mask, goggles, waterproof-gown and a double pair of gloves. Alcohol asepsis was performed on the area to be punctured to obtain the biopsy. The sample was obtained in the first 30 min after death of the patients and of the control subject. The heart, liver, kidney, and lung to be punctured were located by ultrasound using the SONOSCAPE X3 portable ultrasound machine with an X3 sector transducer. The average distance for the biopsy was measured, calculating the depth, which was found to be of 22 mm. The reusable tissue biopsy gun (BARD MAGNUM) was used. The heart was located using a four-chamber apical view with the patient in supine position. It was punctured under direct vision, orienting the disposable needle for biopsy (Magnum MN 1420, 16G x20cm) to the interventricular septum. Three punctures were made, seeking to obtain suitable material for the histological study and each sample was placed in a different bottle with 4% paraformaldehyde, 0.1% glutaraldehyde in 0.1 M PBS pH 7.4. The liver and heart biopsy were performed by placing the ultrasound in the right upper quadrant and mid axillary line, with the patient in supine position. Puncture was performed under direct vision with an average depth of 3 cm. Three samples were taken, trying to obtain adequate material. The renal biopsy was performed in dorsal decubitus at the level of the right flank or in lateral decubitus in the right or left lumbar region. Three punctures were performed seeking to obtain adequate material for the histological study. For the lung biopsy, punctures were performed at the apical, sub clavicular, right, and left lung levels. The biopsy obtention was guided by ultrasound at an average depth of 3 cm. Punctures were also made at the basal level and mid-axillary line of both lungs. A sample was taken from each puncture site.

Electron microscopy

For electron microscopy, small postmortem tissue samples from the lung, heart, kidney cortexes, and liver of patients with COVID-19 and of the control subject were fixed with 2.5% glutaraldehyde for 1 hour and then stored in 0.1M cacodylate buffer. Afterwards they were post-fixed in 1% osmium tetroxide in 0.1M cacodylate buffer (w/v). The samples were dehydrated in a graded series of ethanol and embedded in EPON 812 (Electron Microscopy Sciences). Ultrathin sections (60 nm in thickness) were cut using a Leica Ultracut microtome (RMC pt XL, Boeckeler Instrumentes Inc., Tucson, AZ. USA) mounted on copper grids. Sections were contrasted with 3% uranyl acetate and 0.1% lead citrate and evaluated with a JEM-1011 (JEOL Ltd., Tokyo, Japan) at 80 kV, equipped with AMT 542.391 analysis software.

Immune colloidal gold technique

Small tissue samples of the lung, heart, kidney cortexes, and liver from the postmortem patients that had been infected with COVID-19 and of the control subject were processed according to the immune colloidal gold technique. Briefly, 1 mm tissue pieces were fixed for 2 hours in 4% paraformaldehyde, 0.1% glutaraldehyde in 0.1 M PBS pH 7.4. They were then wash three times with PBS/lysine solution (0.1M sodium phosphate, sodium chloride 0.15 M and lysine 0.10M, pH 7.4) at 4°C for 30 min. afterwards, they were dehydrated with graded series of ethanol at 4°C for 30 min. The infiltration was made progressively with a mixture that consisted of 1:3 and 1:2 ratio of ethanol/LR white for 3 h. They were then washed with LR only for 3 hour, and incubated at 60°C. The samples were cut and mounted on carbon/formvar coated nickel grids. The samples were then incubated with antiserum for 1 hour, and with the primary antibodies dilute 1:20. Nitrotyrosine (HM.11), mouse monoclonal $IgG_{2b,}$ sc-32731 (SantaCruz BioTechnology). COX II (D-5), mouse monoclonal IgM (kappa light chain), sc-514489 (SantaCruz BioTechnology). Anti-COX IV, rabbit polyclonal antibody pAb, VB110-39115 (Wanleibio). Anti-Caspase-9 antibody rabbit polyclonal antibody, ab25758 (abcam). Bcl-2 antibody (N-19) rabbit polyclonal antibody sc-492 (SantaCruz BioTechnology) and anti-MnSOD rabbit polyclonal antibody IgG BIRBORB11394-100 (vwr) in a moist chamber at 4°C overnight The samples were then washed 3 times for 10 min at 24°C, and incubated with secondary antibody conjugated with colloidal gold dilute 1:20 rabbit-anti-mouse gold 25nm cat:25352 (Electron Microscopy Sciences), goat-anti-rabbit gold 15nm cat:25112 (Electron Microscopy Sciences), and Goat Anti-Mouse IgG 10nm Gold, 10 OD, ab270536, (abcam) at 24°C for 3 hrs. They were washed with 0.1 M PBS and fixed with 2% glutaraldehyde. They were stained with 3% uranyl acetate and 0.1 % lead citrate and evaluated with a JEM-1011 (JEOL Ltd., Tokyo, Japan) at 80 kV, equipped with AMT 542.391 analysis software.

Histological sections

For light microscopy, histological small sections of the tissue samples of the postmortem patients of COVID-19 and of the control subject from the lung, left ventricle of the heart, kidney cortexes, and liver were washed in 0.9% NaCl for 30 sec. and fixed by immersion in phosphate buffer with 10% formalin (pH 7.4) for 24 h. The sections were processed according to conventional histological procedures by hematoxylin-eosin (H-E) stain. All photomicrographs were obtained with a Leica DM500 light microscope with objective Plan 10x/0.22 NA and Plan 40/0.065 NA objectives, with digital camera for ICC50W/wi-fi microscope, Leica.

X-ray plates

The conventional X-ray plates were taken from patients with COVID-19 in an anteroposterior position using a mobile portable-X Ray unit (Siemens, Erlangen Germany), together with a digital system (Flat panel).

Statistical Analysis

Measures of central tendency and the normality test (Shapiro-Wilk) were used. Comparison of the independent variables by Mann-Whitney rank sum test, and the paired data using the Wilcoxon sign-rank test. A $p \leq 0.05$ value was considered as statistically significant. The computer program SPSS version 19 (IBM Statistics, Armonk N.Y.), was used.

Results

Demographic characteristics

A total of 15 patients were examined, of which 12 were men (80%) and 3 were women (20%). Patients had an age range of 47-74 years. In them, infection by SARS-CoV-2 was diagnosed through CRP-tests, COVID-19-triage, Reporting and Data System (CO-RADS) and/or the score by computed tomography. The CRP-test was positive in 12 patients. In 3 patients there was not a confirmatory test, in two of them the test result was not collected after the death of the patients and in one the test was negative. However, the pneumonia, the numerous days of the hospital stay and the lack of statistically significant differences in the laboratory test of these 3 patients when compared to patients with positive tests suggest they had COVID-19. Moreover, in the analysis by electron microscopy of the tissues, viral particles were present in tissues from these patients as in the patients with positive tests. The demographic characteristics of the patients are shown in Table 1. The average number of days of hospital stay was 10 days with a minimum of two and a maximum of 35. Only one patient underwent a tracheostomy. During the evolution of the disease, 12 patients had acute renal failure, 2 had pulmonary thromboembolism, one patient had a myocardial infarction, and another had three-vessel ischemic disease with severe aortic and mitral regurgitation. In these last two cases, interventional treatment was warranted. 10 patients received mechanical ventilation, of which in 7 the measure was initiatied at the time of admission, 1 a day later, 1 two days later and 1 three days after admission. 5 patients were only given supplemental oxygen treatment. The characteristics of previous diseases and organ failure and complications during the evolution of infection by SARS-CoV-2, are shows in Table 2.

Therapeutic antiviral management

The treatment applied during hospitalization was, Lopinavir/ritonavir in 5 (33.3%), Lopinavir/ritonavir and angioplasty in 1 (6.7%), ivabradine in 2 (13.3%), tocilizumab in 1 (6.7%), hydrocortisone in 1 (6.7%), amikacin in 1 (6.7%) Levofloxacin in 1 (6.7%), vancomycin in 1 (6.7%) and angioplasty in 1 (6.7%). One patient was treated by a private doctor at home with acyclovir and his death happened on the same day of admission; therefore, he was only treated with resuscitation maneuvers and support medications. In 10 patients (66.6%) the diagnosis was viral pneumonia due to COVID 19 of which, 2 also had cardiogenic shock, 3 had septic shock, 2 ischemic heart diseases and 3 only pneumonia by COVID-19. Community-acquired pneumonia and septic shock was present in 2 (13.3%). 1 adult (13.3%) had respiratory distress syndrome and 1 patient was diagnosed with cardiogenic shock and acute myocardial infarction with suspected SARS-CoV-2 infection.

Laboratory levels

Table 3 shows the laboratory results on admission and at the time of death for the COVID-19 patients. Many of the patients were already showing changes in the different basal blood parameters when they were admitted, $p \leq 0.03$.

X-ray plates

The results of the representative X-ray plates are shown in Fig. 1A, B, C and D. These alterations were related with the histopathological changes in the lung Fig. 1E. In the lung samples, there are changes corresponding to pneumonitis with increased thickness of the alveolar walls, capillary congestion, and hyperplasia of pneumocytes.

Histology

The histological results of the patients with COVID-19 were compared with a control subject which was 60-year-old female patient, who showed mild changes of cardiac hypertrophy with variability in the size and shape of the nuclei some with hyperchromatism (Fig. 2A). In COVID-19 patients, the changes in cardiac hypertrophy are more marked as may can observed in Fig. 2B. In the liver, patients having COVID-19 show preserved morphology, but there is a slight increase in the inflammatory infiltrate by lymphocytes in the portal spaces show an increase in fibro connective tissue. There is steatosis, and congestion in the sinusoids (Fig. 2C and D).

Electron microscopy

The results of the electron microscopy of the heart and liver are shown in Fig. 3A, B and lung are shown in Fig. 3C and D, respectively.

Immune colloidal gold technique

The results of the immune colloidal gold marker showed that COX II and IV were present in the cytosol, outside and inside the mitochondrial outer matrix of the heart tissue from COVID-19 patients, Fig. 4B and D. Furthermore, the mitochondrias lacked the normal mitochondrial structural integrity. In comparison, the colloidal gold marker was present inside the mitochondrial matrix in the control subject (Fig. 4A, and C respectively). Fig. 4F show that the immune colloidal marker for MnSOD was present outside and inside the mitochondrias in the samples from COVID-19 patients. In comparison, the mark was only found inside mitochondria in control subject Fig. 4E.

Fig. 5A and B show the immune colloidal marker for nitrotyrosine was present outside and inside the mitochondrias in the samples from COVID-19 patients Fig. 5B. In comparison, the mark was only found inside mitochondria in control subject Fig. 5A. The Fig. 5C, and D show the immune colloidal marker for caspase 9 and Fig. 5 E and F show the immune colloidal marker for Bcl-2 respectively. The mark was found inside the mitochondrias in samples from COVID-19 patients. In comparison, electrodense zones were not present in the control subject.

Discussion

Mitochondrial defects have been implicated in numerous pathologies including diabetes, cardiovascular diseases, gastrointestinal disorders, cancer, and aging (Melser et al., 2015). Studies of these diseases indicate that elevated glucose concentrations may significantly alter the resting bioenergetics state associate with a reduction in mitochondrial respiration, compromised ATP turnover, proton leak, and mitochondrial uncoupling (Rumora et al., 2018). Mitochondria can also play an important role in viral infections, and there is normally a mitochondrial evasive response and one of the first steps that the viruses perform after it invades the host cells is the disruption of the mitochondrial function. Although it has been suggested that SARS-CoV-2 hinders mitochondrial functioning, there is still no proof of its effects (Jean-Beltran et al., 2017). Therefore, the aim of this study was to show that the virus kidnaps the mitochondrial machinery for its benefit and survival. To prove this, we show that mitochondrial morphology is altered and that there is rupture of these organelles and presence of the viral particles in the mitochondrial matrix in COVID-19 patients, and which no is present in control subject. We show larger changes of cardiac hypertrophy and variability in the size and shape of the nuclei with some hyperchromatism and some changes in the mitochondria in patients with SARS-CoV-2, in comparison with control subject who showed mild alterations. Many of the enzymes normally present inside the mitochondria are found in the cytoplasm of cells of different tissues from patients who died from COVID-19. Substrates and products from mitochondrial functions are altered in the serum of patients as a consequence of mitochondrial dysfunction and this may lead to multiorgan failure.

The results from our series of patients show that serum Ca^{2+} levels were low since admission and Ca^{2+} homeostasis was altered in mitochondria, ER and Golgi apparatus. The flux of Ca^{2+} released from ER and utilized by mitochondria can boost ATP production to meet a higher demand for energy due to constant viral replication. However, later on, there is a decrease in the Ca^{2+} concentration both in the ER and Golgi apparatus which may contribute to inhibit protein trafficking pathways, decrease the antiviral response of the host, and preventing premature elimination by IFNs and the immune system (Zhou et al., 2009). This suggests that the control of the Ca^{2+} homeostasis by SARS-CoV-2, could constitute an important target particularly preventing the activation of apoptotic checkpoints to prevent host immune clearance and promote virus replication. This same mechanism has been described for other viruses (Davies et al., 2020).

On the other hand, iron-sulfur proteins (ISP) constitute a family of electron transporters in the ETC. There are at least 6 iron-sulfur centers, in addition to cytochromes. These proteins have a heme group, consisting of a porphyrin ring and an iron atom those changes from state III to state II each time it accepts an electron. Cytochrome C is an essential component of the ETC transferring electrons from complex III to complex IV. It plays a key role in the early events of mitochondria-mediated apoptosis (Sakaida et al., 2005). In addition, serological findings in critically ill COVID-19 patients with coagulopathy and thrombocytopenia show the presence of anticardiolipin IgA antibodies in serum. The presence of anticardiolipin IgA antibodies suggests mitochondrial impairments associated with COVID-19. Cardiolipin is a mitochondrial phospholipid which participates in the maintenance of the structural integrity of the mitochondrial membrane where the proteins that make up the ETC are anchored (Zhang et al., 2020). The loss of structural integrity of the mitochondrial membrane may lead to release to the cytosol of ISP and cytochrome C. When

the cytochrome C is released from the mitochondrial intermembrane space, it induces the activation of caspases (Malgorzata et al., 2020).

The results by immune colloidal gold marker show that COX II and IV were found in the cytosol and outside the mitochondrial outer matrix. There was also a lack of mitochondrial structural integrity. Furthermore, the liberation of the ISP and heme group of the cytochromes can contribute to the iron deregulation manifested as hyperferritinemia in COVID-19 patients. Iron deregulation induces the production of reactive oxygen species (ROS) by the Fenton-Haber Weiss reaction and promotes oxidative stress (Pérez-Torres et al., 2020). Both the iron overload and high concentrations of ROS may be involved in platelet receptor activation that can result in platelet dysfunction and high thrombosis (García-Yébenes et al., 2018). Appropriate mitochondrial functioning relies, in part, on iron uptake that is primarily utilized for storage in mitochondrial ferritin, in the iron-sulfur cluster biogenesis and in the heme group synthesis (Paul et al., 2017). Hence, disruption of cellular iron levels or mitochondrial iron metabolism can result in cellular stress or death. The hyperferritinemia observed in the COVID-19 patients may be attributed to high levels of ferritin which, in turn, may cause elevated oxidative and cellular stress that leads to massive release of inflammatory mediators and free radicals (Edeas et al., 2020). Also, the hyperferritenimia is highlighted as a predictor of increased mortality of the disease (Delgado-Roche and Mesta, 2020). In addition, the hyperferritinemia can lead to a change in mitochondrial respiration from an aerobic into an anaerobic state. In this condition, pyruvate reduction into lactate is favored. This leads to an increase of the lactate dehydrogenase, which is a highly up regulated marker in COVID-19 (Young et al., 2020).

The results in this series of COVID-19 patients show that lactate was increased since admission and remained high. This might reflect the degree of the anaerobic state in the mitochondria. Consequently, anaerobic mitochondria can result in a diminished cellular respiratory function as has been shown in cardiac myocytes with excess iron loading. Dysfunctional mitochondria would result in iron accumulation due to their incapacity to metabolize it. This might cause a deficient iron sequestration, leading to ROS (Lane et al., 2015). In addition, an increase in lactate production in HCV-infected cells, has been demonstrate, due to kidnapping of the mitochondrial function by the virus, which then provokes an increased dependency on glycolysis in the hepatocyte to support the energy needs (Ramiere et al., 2014).

Mitochondrial involvement in the viral survival is relevant since viruses require a source of energy to favor the active processes involved in their life cycle (Glingston et al., 2019). Some viruses modulate the normal cells metabolism to increase aerobic glycolysis and use glucose from bio-synthetical processes, which helps viruses to increase the available pool of fatty acids and nucleotides during their replication (Kapadia et al., 2005).

Our results show that plasma glucose levels were increased since admission in this series patient with COVID-19, and levels remained high until the fatal outcome. This suggests that SARS-CoV-2 may increase aerobic glycolysis which can contribute and favor the increase the glucose in blood. Besides, the increase in lactate is favored by a limiting rate of the available oxygen in a hypoxic state. In addition, an environment rich in glucose can favor an imbalance in the electron gradient coming from the ETC, which leads to an increase in ROS (Herst et al., 2017).

Several stages of the coronavirus replication cycle are closely associated with ER and mitochondrial stress. Indeed, expression of several coronavirus proteins, including the heavily glycosylated S protein, induces ER stress, which is observed in coronavirus-infected cells (Chan et al., 2006). Furthermore, the cytokines storm can induce a Ca^{2+}-dependent increase in the mitochondrial ROS, creating a positive feedback loop, which may directly unbalance the activity of the ETC, stimulating the production of proinflammatory cytokines (Li et al., 2013). This may cause mitochondrial membrane permeabilization, altered mitochondrial dynamics, and might ultimately result in cell death by apoptosis (Mittal et al., 2014). Also, an increase in ROS can be subsequently accompanied by reduced mitochondrial manganese which may result in mitochondrial dysfunctions, mainly in a low activity or expression of MnSOD, an enzyme that protects the mitochondria from the ROS that are generated by the respiratory process (Jouihan et al., 2008). The results in this study show that the localization of the MnSOD was not within the mitochondria, but outside it. This suggests that this enzyme may not be playing an adequate function in the detoxification of the ROS, and this can lead to a process of oxidation of mitochondrial proteins.

Regarding the damage to proteins, it might be caused by the virus S-nitrosylation resulting from an excess in the production of $ONOO^-$. This molecule is a secondary metabolite of the oxidation of nitric oxide, and its presence is associated with

overproduction by the inducible nitric oxide synthase in a state of the chronic inflammation such as is present in COVID-19 (Pérez-Torres et al., 2020; Soto et al., 2020). $ONOO^-$ may inactivate different mitochondrial proteins, including ETC components and citric acid cycle dehydrogenases and this may contribute to inactivation decreasing the ATP levels (Pérez-Torres et al., 2020). Our results show that the localization of the labeling of S-nitrosylation proteins occurs both inside and outside of the mitochondria. This suggests that in COVID-19 patients, there is presence of NSS, probably resulting from the chronic inflammation associated to the cytokine storm.

Mitochondria actively communicate with the cytosol and nuclear compartments. Proteins located in the mitochondrial membrane, including the mitochondrial permeability transition pore (MPTP) help in the signaling involved in this communication process (Kwong and Molkentin, 2015). The products from the action of the ETC, such as ATP and cytochrome C, are transferred to the cytosol to exert their biological functions through the MPTP and many viral proteins may alter the MPTP (Williamson et al., 2012). Altering the MPTP leads to passive swelling, outer membrane rupture, osmotic water flux, and release of pro-apoptotic factors leading to cell death (Anand and Tikoo, 2013). For example, HCV can induce the MPTP opening, regulating the release of mitochondrial contents such as mitDNA and cytochrome C (Rongvaux et al., 2014). Furthermore, in an oxidative stress condition or cell damage by infection, mitDNA leaks out into the cytoplasm and once in the outside, it triggers inflammation and anti-viral responses, which involve the AIM2 and/or endosomal/extracellular toll-like receptor 9 (Mills et al., 2017). However, the liberation of the mitDNA levels and cytochrome C increase the severity and progress of the infection and correlate with the onset of multiorgan failure in patients affected by acute respiratory distress (Simmons et al., 2017). This suggests that the SARS-CoV-2 can manipulate the release of mitDNA and cytochrome C, which participate in the inflammation process (Singh et al., 2020). The release the cytochrome C results in permeabilization of the mitochondrial membrane, activation of caspases and apoptosis. Different virus may activate the caspases cascade and lead to an increase in apoptosis (Roshal et al., 2001). These processes are indispensables for killing the infected cells during the viral replication phase (Guler et al., 2020).

Our results show that labeling of caspase 9 occurred in the mitochondria. However, in the eagerness of the host cell to protect itself from this increase in the apoptotic process, the host tries to activate alternative protective metabolic pathways such as the expression of the protein Bcl-2 (Luna-López et al., 2008). The Bcl-2 protein is a 26 kDa protein that is anchored to the outer membranes of the nuclear cisterns, the ER, and the outer membrane of the mitochondria. It is anchored to the mitochondrial membrane is linked to anti-apoptotic properties. Bcl-2 participates in the preservation of the integrity of the mitochondrial membrane and in the prevention of the release of cytochrome C and of the activation of the caspases cascade. In addition, the expression of this protein can decrease the levels of $ONOO^-$ during periods of oxidative stress and stimuli that generate apoptosis (Luna-López et al., 2008).

Our results show that the localization of the labeling of Bcl-2 occurred in the mitochondria. This suggests that Bcl-2 expression is a mechanism of host protection to decrease the apoptotic process and oxidizing background. In addition, the localization of the nitrotyrosine labeling that appeared in the outer and inner membrane of the mitochondria suggests that infection by SARS-CoV-2 may induce NSS associated to the increase in hyperferritinemia that results from the release of cytochrome C and ISP. This also contributes to the expression of Bcl-2. In addition, the apoptotic process is a trigger of the elevation of the D-dimer in COVID-19 patients (Guler et al., 2020). The results show, the D-dimer, troponin, and fibrinogen were increase from admission and their levels remained high until the fatal outcome. The fibrinogen and troponin increase can be due to the double protective function it plays, regulating the antiviral function of the immune cells, and assisting the host protective formation of fibrin matrices or clots that serve as a protective barrier that limits the spread of the virus (Thachil et al., 2020). However, this condition results in coagulation abnormalities that are associated with a substantial COVID-19 mortality rate (Levi et al., 2020).

On the other hand, the mitochondrial life cycle is comprised of frequent fusion (in which two mitochondria form a single organelle) and fission (the division of one mitochondrion into two daughter organelles) events. These two opposing processes collaboratively control the number and size of mitochondria and maintain cell homeostasis (Wang et al., 2017). Mitochondrial fusion helps in exchanging matrix metabolites and in the preservation of mitochondrial DNA. Mitochondrial fission helps in sorting impaired mitochondria from the healthy population which are further eliminated by a process called mitophagy (Anand, and Tikoo, 2013). The equilibrium between fission and fusion is crucial for the stabilization of mitDNA (Bernhardt et al., 2015). Upon viral infection, the above dynamic events are altered in order for the virus to facilitate its replication. For example, the ORF-

9B protein of SARS-CoV virus promotes mitochondrial fusion in HEK293 cells (Anand, and Tikoo, 2013). The infection by HCV in hepatocytes can be result in the fission and fusion processes which are responsible for the exchange and reallocation of mitochondrial contents including mitDNA depletion (Wai and Langer, 2016). The results from the ultrastructural mitochondrial analysis in this study show that these organelles are undergoing fusion. In addition, the ultrastructural changes observed in the COVID-19 patients and the control subject do not correspond to postmortem alterations per se of the tissue, because the time to obtain the biopsies was short, so these alterations may be typical of the infection by SARS-CoV-2. Also, the ultrastructural changes in the control subject are typical of the pathology that with which the subject was coursing and do not correspond to the changes observed in COVID-19 patients. This suggests that the host cells, to protect themselves from kidnapping by the SARS-CoV-2, trigger these processes in the mitochondria.

Mitochondrial morpho dynamics can also regulate the respiratory rate, and constitutes a strategy used by SARS-CoV-2 to corrupt mitochondrial metabolism to evade the immune response (Khan et al., 2015). This condition, in addition to the other mitochondrial alterations already mentioned, may increase in NDUFS2 that regulates oxygen-sensitive potassium and voltage-gated Ca^{2+} channels initiating hypoxic a pulmonary vasoconstriction in the lungs rendering them stiff and fibrotic. Hyaline membranes in the alveoli are a prominent feature of lungs from patients with COVID-19, and dyspnea is profound (Archer et al., 2020). It is evident in the X-ray plates and by histopathological changes in lung tissue in our series of patients.

The inadequate cellular O_2 supply can result in alterations in the tricarboxylic acid cycle and uncoupling of the ETC, leading to a decrease in the proton gradient (Levy and Deutschman, 2007), which results in production of heat rather than the generation of ATP (Brealey et al., 2002), this could may contribute to increase the temperature in COVID-19 patients.

Septic circulatory shock, the development of a cytokine storm and the severe and irreversible damage found in COVID-19 patients, may also be the result of an excessive production of ammonia (greater than 1mm). Ammonia is usually produced by the urea cycle and the dysfunction of this cycle leads to its excess. The urea cycle comprises five reactions and allows the transformation of ammonia into urea that is then eliminated in the urine. Six enzymes participate in this catalysis: N-acetyl-glutamate synthetase, carbamoyl-phosphate synthetase, ornithine transcarbamylase, argino-succinate synthetase, argino-succinate lyase and arginase. The first three enzymes are located in the mitochondria and the last one in the cytosol. Despite the hepatic location of the complete cycle, which renders the liver the main center for elimination of ammonia toxicity, the six enzymes are also present in other tissues. Although the activity of the urea cycle depends mainly on these six enzymes, ammonia is also produced by other enzymatic systems such as transport systems in the mitochondrial membrane that allow the exchange of aspartate-glutamate and citrulline-ornithine (Levy et al., 2003). The results from this series of patients, we found that both aspartate amino transferase (ASAT/GOT) and alanine amino transferase (AAT/GPT) were increased since admittance of the patients, without there being a statistical difference between the levels at admission and those that at the time of death. This indicates that the infected patients have persistent liver failure, which may be associated with the inability to detoxify ammonia. Furthermore, these patients showed elevated levels of urea nitrogen since their admission and they showed a statistically significant increase according to the differential delta observed p=0001 at the time of death. This may be due to poor blood flow distribution and low peripheral vascular resistance, especially at the microcirculatory level, which in turn results from inflammation and endotoxemia (Ince, 2005).

The results show that albumin was decreased. The mean value found at admission and compared with that of the final state of the patient, showed a considerable statistically significant delta (p=0.001). This confirms that in patients with sepsis, there is nutritional deterioration which progresses rapidly. The elevated level of CRP found at admission remained elevated until the time of death. Therefore, it did not show a delta difference and the same was found with ferritin. CRP is produced in the liver and rises when there is a severe inflammatory state. Nevertheless, this enzyme also rises when there is liver disease due to alcohol abuse, hemochromatosis, liver cirrhosis, heart disease and diabetes. It is also worth noting that in the case of a persistent inflammatory state, an increase in fibrinogen is found. Fibrinogen, like CRP and ferritin, is an acute phase reactant of inflammation and it showed an increase during evolution of the patients in this series, having a statistical significance. Although the inflammatory state is relevant in these patients, the most relevant data was the deterioration of renal function. This was demonstrated by the increase in serum creatinine and urea nitrogen, which goes hand in hand with the elevation of inflammation markers from the liver and impaired mitochondrial function.

Conclusions

The multiorganic dysfunction present in COVID-19 patients may be in part due to damage to the mitochondria's that result in an inflammatory state. Mitochondrial damage renders dysfunctional these organelles and they are unable to meet the hyper metabolic demands associated with the sepsis caused by SARS-CoV-2. The alteration of the mitochondrial proteins can result in damage that inactivates innate immunity. Also, these alterations contribute to the elevation of ROS and NSS that activates the sepsis cascade. The hyper inflammatory state and the deregulation of the OS contribute to the increased mortality linked to sepsis by COVID-19. Also, the results of this study indicate an interplay between SARS-CoV-2 and mitochondrial dysfunction leading to sepsis that is associated with death of the patients. Figure 6 and 7 describes the kidnapping of the mitochondrial function and damage associated to SARS-CoV-2 infection.

Perspectives

The results observed in this study suggest that many of the alteration in the mitochondria can be decreased by a combined therapeutic strategy (Soto et al., 2020). The first phase of this strategy would be to lower the viral load that is the source and origin of the chronic inflammatory condition leading to severe sepsis, multiple organ failure and mitochondrial damage. The second phase should be aimed to decrease alterations in the mitochondria which may be lowered by the use of antioxidants such as melatonin and N-acetyl-cysteine that have the capacity of restoring and protecting the mitochondrial function [Soto et al., 2020; Aisa-Alvarez et al., 2020). In addition, the use of direct-acting antivirals, in particular, the nucleoside/nucleotide analogues such as the remdesivir can efficiently inhibit viral replication by inhibiting the viral polymerase activity. However, these drugs may exert off-target effects by inhibition of mitochondrial DNA polymerase, resulting in a reduction of mitDNA copy number (Qu et al., 2019).

Study limitations

The main limitation of this study was the obtainment of postmortem samples from patients with COVID-19. The technique of obtaining biopsies through an ultrasound-guided technique is minimally invasive and very specific; however, it is not possible to take biopsies of all organs or tissues and it is particularly complicated to take samples from the brain or the bone. It is not possible to perform a complete autopsy in patients that died from COVID-19 due to the risk that this implies to the health personnel.

Declarations

Data Availability: The datasets generated and analyzed during the current study are available from the corresponding author on reasonable request.

Author Contributions: E.S-C. Made the immunogold, captured the electron micrographs and the description of the images, I.P.-T. Designed the study, and wrote the paper, M.E.S. analyzed the clinical record and the designed the tables. V.G.-L. wrote and restructured the manuscript. G.R. performed the postmortem samples; M.P.D. performed the histological description. S.A.C.-V. performed X-ray plaques and description L.M.P. performed the figures. All authors have read and agreed to the published version of the manuscript.

Funding: This research received no external funding

Acknowledgments: We thank Rocio Torrico-Lavayen for electron microscopy histological technical support, and Benito Chávez Rentería for histology technical support. We thank to Vicente Castrejón-Tellez and Mohammed El Hafidi for providing us with the antibodies against Bcl-2, caspase 9, COX II and nitrotyrosine.

Conflicts of Interest: The authors declare no conflict of interest.

References

Aisa-Alvarez A., Soto M.E., Guarner-Lans V., Camarena-Alejo G., Franco-Granillo J., Martínez-Rodríguez E.A., Gamboa Á.R., Manzano-Pech L. and Pérez-Torres I. (2020). Usefulness of antioxidants as adjuvant therapy for septic shock: A randomized clinical trial. Medicina (Kaunas). 56, 619.

Anand S.K. and Tikoo S.K. (2013). Viruses as modulators of mitochondrial functions. Adv. Virol. 2013, 738794.

Archer S.L., Sharp W.W. and Weir E.K. (2020). Differentiating COVID-19 pneumonia from acute respiratory distress syndrome and high altitude pulmonary edema: Therapeutic implications circulation. Circulation. 142, 101-104.

Bernhardt D., Muller M., Reichert A.S. and Osiewacz H.D. (2015). Simultaneous impairment of mitochondrial fission and fusion reduces mitophagy and shortens replicative lifespan. Sci. Rep. 5, 7885.

Brealey D., Brand M., Hargreaves I., Heales S., Land J., Smolenski R., Nathan A.D., Chris E.C. and Mervyn S. (2002). Association between mitochondrial dysfunction and severity and outcome of septic shock. Lancet. 360, 219-223.

Chan C.P., Siu K.L., Chin K.T., Yuen K.Y., Zheng B. and Jin D.Y. (2006). Modulation of the unfolded protein response by the severe acute respiratory syndrome coronavirus spike protein. J. Virol. 80, 9279-9287.

Davies J.P., Almasy K.M., McDonald E.F. and Plate, L. (2020). Comparative multiplexed interactomics of SARS-CoV-2 and homologous coronavirus non-structural proteins identifies unique and shared host-cell dependencies. bioRxiv. 2020, 201517.

Delgado-Roche L. and Mesta F. (2020). Oxidative stress as key player in severe acute respiratory syndrome Coronavirus (SARS-CoV) Infection. Arch. Med. Res. 51, 384-387.

Edeas M., Jumana S. and Peyssonnaux, C. (2020). Iron: innocent bystander or vicious culprit in COVID-19 pathogenesis? Int. J. Infect. Dis. 97, 303-305.

García-Yébenes I., García-Culebras A., Peña-Martínez C., Fernández-López D., Díaz G.J., Negredo P., Avendaño C., Castellanos M., Gasull T., Dávalos A., Moro M.A. and Lizasoain I. (2018). Iron overload exacerbates the risk of hemorrhagic transformation after TPA (tissue-type plasminogen activator) administration in thromboembolic stroke mice. Stroke. 49, 2163-2172.

Glingston S.R., Deb R., Kumar S. and Nagotu S. (2019). Organelle dynamics and viral infections: at cross roads. Microbes. Infect. 21, 20-32.

Guler N., Siddiqui F. and Fareed, J. (2020) Is the reason of increased D-Dimer levels in COVID-19 because of ACE-2-induced apoptosis in endothelium? Clin. Appl. Thromb. Hemost. 26, 1076029620935526.

Hee J.S. and Cresswell P. (2017). Viperin interaction with mitochondrial antiviral signaling protein (MAVS) limits viperin-mediated inhibition of the interferon response in macrophages. PLoS. One. 12, e0172236.

Herst P.M., Rowe M.R., Carson, G.M. and Berridge M.V. (2017). Functional mitochondria in health and disease Front. Endocrinol. (Lausanne). 8, 296.

Ibrahim I.M., Abdelmalek D.H., Elshahat M.E. and Elfiky, A.A. (2020). COVID-19 Spike-host cell receptor GRP78 binding site prediction. J. Infect. 80, 554-562.

Ince C. (2005). The microcirculation is the motor of sepsis. Crit. Care. 9, S13-S19.

Jean-Beltran P.M., Cook K.C. and Cristea I.M. (2017). Exploring and exploiting proteome organization during viral infection. J. Virol. 91, e00268-e00217.

Jonathan P.D., Almasy K.M., Eli F.M. and Lars P. (2020). Comparative multiplexed interactomics of SARS-CoV-2 and homologous coronavirus non-structural proteins identifies unique and shared host-cell dependencies. bioRxiv. 2020, 201517.

Jouihan H.A., Cobine P.A., Cooksey R.C., Hoagland E.A., Boudina S., Abel E.D., Winge D.R. and McClain D.A. (2008). Iron-mediated inhibition of mitochondrial manganese uptake mediates mitochondrial dysfunction in a mouse model of hemochromatosis. Mol. Med. 14, 98-108.

Kapadia S.B. and Chisari F.V. (2005). Hepatitis C virus RNA replication is regulated by host geranylgeranylation and fatty acids. Proc. Natl. Acad. Sci. U S A. 102, 2561-2566.

Khan M., Syed G.H., Kim S.J. and Siddiqui, A. (2015). Mitochondrial dynamics and viral infections: a close nexus. Biochim. Biophys. Acta. 1853, 2822-2833.

Koshiba T., Yasukawa K., Yanagi Y. and Kawabata S. (2011). Mitochondrial membrane potential is required for MAVS-mediated antiviral signaling. Sci. Signal. 158, ra7.

Kwong J.Q. and Molkentin J.D. (2015). Physiological and pathological roles of the mitochondrial permeability transition pore in the heart. Cell. Metab. 21, 206-214.

Lane D.J.R., Merlot A.M., Huang M.L.H., Bae D.H., Jansson, P.J., Sahni, S., Kalinowski D.S. and Richardson D.R. (2015). Cellular iron uptake, trafficking and metabolism: key molecules and mechanisms and their roles in disease. Biochim. Biophys. Acta. 1853, 1130-1144.

Levi M., Thachil J., Iba T. and Levy J.H. (2020). Coagulation abnormalities and thrombosis in patients with COVID-19. Lancet. Haematol. 6, e438-e440.

Levy M.M., Fink M.P., Marshall J.C., Abraham E., Angus D., Cook D., Cohen J., Opal SM., Vincent S.M. and Ramsay J.L. (2003). 2001 SCCM/ESICM/ACCP/ATS/SIS international sepsis definitions conference. Crit. Care. Med. 31, 1250-1256.

Levy R.J. and Deutschman C.S. Cytochrome c oxidase dysfunction in sepsis. (2007). Crit. Care. Med. 35, S468-S475.

Li X., Fang P., Mai J., Choin E.T., Wang H. and Yang X.F. (2013). Targeting mitochondrial reactive oxygen species as novel therapy for inflammatory diseases and cancers. J. Hematol. Oncol. 6, 19.

Lu L.F., Li S., Lu X.B., LaPatra S.E., Zhang N., Zhang X.J., Chen D.D., Nie P. and Zhang Y.A. (2016). Spring viremia of carp virus N protein suppresses fish IFNφ1 production by targeting the mitochondrial antiviral signaling protein. J. Immunol. 196, 3744-3753.

Luna-López A., López-Diazguerrero N.E., González-Puertos V.Y., Triana-Martínez F. and Königsberg-Fainstein M. (2008). El fantástico mundo de la proteína Bcl-2. Reb. 27, 93-102.

Mailloux R.J. (2018). Mitochondrial antioxidants and maintenance of cellular hydrogen peroxide levels. Oxid. Med. Cell. Longev. 2018, 1-10.

Malgorzata K., Ghobrial R.M. and Kubiak J.Z. (2020). The Role of genetic sex and mitochondria in response to COVID-19 infection. Int. Arch. Allergy. Immunol. 181, 629-634.

Melser S., Lavie J. and Bénard G. (2015). Mitochondrial degradation and energy metabolism. Biochim. Biophysi. Acta. 1853, 2812-2821.

Mills E.L., Kelly B. and O'Neill L.A.J. (2017). Mitochondria are the powerhouses of immunity. Nat. Immunol. 18, 488-498.

Mittal M., Siddiqui M.R., Tran K., Reddy S.P. and Malik A.B. (2014). Reactive oxygen species in inflammation and tissue injury. Antioxid. Redox. Signal. 20, 1126-1167.

Paul B.T., Manz D.H., Torti F.M. and Torti S.V. (2017). Mitochondria and Iron: current questions. Expert. Rev. Hematol. 10, 65–79.

Paumard P.J., Vaillier J., Coulary B., Schaeffer J., Soubannier V., Mueller D.M., Brèthes D., di Rago J.P. and Velours J. (2002). The ATP synthase is involved in generating mitochondrial cristae morphology. EMBO. J. 21, 221-230.

Pérez-Torres I., Manzano-Pech L., Rubio-Ruíz M.E., Soto M.E. and Guarner-Lans, V. (2020). Nitrosative stress and its association with cardiometabolic disorders. Molecules. 25, 2555.

Petersen J.M., Her L.S. and Dahlberg J.E. (2001). Multiple vesiculoviral matrix proteins inhibit both nuclear export and import. Proc. Natl. Acad. Sci. U S A. 98, 8590–8595.

Qu C., Zhang S., Li Y., Wang Y., Peppelenbosch M.P. and Pan Q. (2019). Mitochondria in the biology, pathogenesis, and treatment of hepatitis virus infections. Rev. Med. Virol. 29, e2075.

Ramiere C., Rodriguez J., Enache L.S., Lotteau V., Andre P. and Diaz O. (2014). Activity of hexokinase is increased by its interaction with hepatitis C virus protein NS5A. J. Virol. 88, 3246-3254.

Rongvaux A., Jackson R., Harman C.C., Li T., West A.P., R de Zoete M., Wu Y., Yordy B., Lakhani S.A. and Kuan C.Y. (2014). Apoptotic caspases prevent the induction of type I interferons by mitochondrial DNA. Cell. 159, 1563-1577.

Roshal M., Zhu Y. and Planelles, V. (2001). Apoptosis in AIDS. Poptosis. 6, 103-116.

Rumora A.E., Lentz S.I., Hinder L.M., Jackson S.W., Valesano A., Levinson G.E. and Feldman E.L. (2018). Dyslipidemia impairs mitochondrial trafficking and function in sensory neurons. FASEB. J. 32, 195–207.

Sakaida I., Kimura T., Yamasaki T., Fukumoto Y., Watanabe K., Aoyama M. and Okita K. (2005). Cytochrome c is a possible new marker for fulminant hepatitis in humans. J. Gastroenterol. 40, 179-185.

Simmons J.D., Lee Y.L., Pastukh V.M., Capley G., Muscat C.A., Muscat D.C., Marshall M.L., Brevard S.B. and Gillespie M.N. (2017). Potential contribution of mitochondrial DNA damage associated molecular patterns in transfusion products to the development of acute respiratory distress syndrome after multiple transfusions J. Trauma. Acute. Care. Surg. 82, 1023-1029.

Singh K.K., Chaubey G., Chen J.Y. and Suravajhala P. (2020). Decoding SARS-CoV-2 hijacking of host mitochondria in COVID-19 pathogenesis. Am. J. Physiol. Cell. Physiol. 319, C258-C267.

Singhal A.T. (2020). Review of coronavirus disease-2019 (COVID-19). Indian. J. Pediatr. 87, 281-286.

Soto M.E., Guarner-Lans V., Soria-Castro E., Manzano-Pech L. and Pérez-Torres I. (2020). Is Antioxidant therapy a useful complementary measure for Covid-19 treatment? An algorithm for its application. Medicina. (Kaunas). 56, E386.

Thachil J. (2020). The protective rather than prothrombotic fibrinogen in COVID-19 and other inflammatory states. J. Thromb. Haemost. 18, 1849-1852.

Wai T. and Langer T. (2016). Mitochondrial dynamics and metabolic regulation. Trends. Endocrinol. Metab. 27, 105-117.

Wang Y.J., Pan Q.W. and Zhao J.M. (2017). Hepatitis E virus infection induces mitochondrial fusion to facilitate viral replication. Hepatology. 66, 372a.

Williamson C.D., DeBiasi R.L. and Colberg-Poley A.M. (2012). Viral product trafficking to mitochondria, mechanisms and roles in pathogenesis. Infect. Disord. Drug. Targets. 12, 18-37.

Wu K.E., Fazal F.M., Parker K.R., Zou J. and Chang H.Y. (2020). RNA-GPS Predicts SARS-CoV-2 RNA residency to host mitochondria and nucleolus. Cell. Syst. 11, 102-108.

Yin X., Li X., Ambardekar C., Hu Z., Lhomme S. and Feng Z. (2017). Hepatitis E virus persists in the presence of a type III interferon response. PLoS. Pathog.13, e1006417.

Young A., Oldford C. and Mailloux R.J. (2020). Lactate dehydrogenase supports lactate oxidation in mitochondria isolated from different mouse tissues. Redox. Biol. 28, 1-7.

Zhang Y., Xiao M., Zhang S., Xia P., Cao W., Jiang W., Chen H., Ding X., Zhao H., Zhang H., Wang C., Zhao J., Sun X., Tian R., Wu W., Wu D., Ma J., Chen Y., Zhang D., Xie J., Yan X., Zhou X., Liu Z., Wang J., Du B., Qin Y., Gao P., Qin X., Xu Y., Zhang W., Li T., Zhang F., Zhao Y., Li Y. and Zhang S. (2020). Coagulopathy and antiphospholipid antibodies in patients with Covid-19. N. Engl. J. Med. 382, e38.

Zhou Y., Frey T.K. and Yang J.J. (2009). Viral calciomics: Interplays between Ca2+ and virus. Cell. Calcium. 46, 1-17.

Tables

Table 1. Demographic Characteristics of the COVID-19 patients

Age	47-74
body mass index	28.6 ± 4.3
Weight by body mass index (%)	
Normal	4 (26.7)
Overweight	6 (40)
Morbid Obesity	5 (33.3)
Habits (%)	
Sedentarism	12 (80)
Alcoholism	5 (33.3)
Smoking	4 (26.7)
Marijuana use	1 (6.7)
Comorbid conditions prior to SARS-CoV-2 (%)	
Diabetes Mellitus	9 (60)
Systemic arterial hypertension	5 (33.3)
Ischemic heart disease	4 (26.7)
Dyslipidemia	3 (20)
Hypothyroidism	1 (6.7)
With valve prosthesis	1 (6.7)
Autoimmune disease (Systemic Lupus Erythematous)	1 (6.7)
Symptoms at the time of hospital admission (%)	
Dyspnea	13 (86.7)
Fever	12 (80)
Cough	7 (46.7)
Asthenia and adynamia	7 (46.7)
Myalgia	6 (40)
Arthralgia	5 (33.3)
Shaking chills	3 (20)
Odynophagia	3 (20)
Headache	3 (20)
Thoracic pain	2 (13.3)
Runny nose	2 (13.3)
Drowsiness	2 (13.3)
Diarrhea	1 (6.7)
dysuria and polyakiuria	1 (6.7)

alues indicate the number of patients having the condition and number in parenthesis represents the percentage of atients showing the condition. The informed consent for the publication of the data was obtained from participants egal guardian(s)/legally authorized representative/next of kin (for dead patients).

Table 3. Laboratory levels on admission and at the moment of death of patients

Reference value units	Laboratory at the admission	Laboratory at the death	p
	Median (Min-Max)	Median (Min-Max)	
Hemoglobin (11.7-16.3 g/dL)	14.5 (10 - 17.4)	**10.8 (7.6 - 16.4)**	**0.001**
Leucocytes (3.56-10.310^3/µL)	11,146 (4600 - 19900)	**16173 (6400 - 25300)**	**0.03**
Lymphocytes (0.99-3.2410^3/µL)	600 (100 - 1900)	600 (200 - 2100)	0.79
Platelets (150000-50000010^3/µL)	218000 (136000 - 314000)	188,000 (113000 - 488000)	0.91
ASAT/GOT (13-39 U/L)	53.5 (6.5 - 131.2)	57.2 (13.5 - 549)	0.68
AAT/GPT (7-52 U/L)	36.7 (14 - 98)	41.5 (14 - 113)	0.97
Creatinine (0.6-1.2 mg/dL)	1.1 (0.40 - 2.1)	**3.1 (0.79 - 7.15)**	**0.001**
Blood urea nitrogen (7-25 mg/dL)	29 (12 - 55.4)	**75.5 (19.25 - 256)**	**0.001**
Glucose (70-105 mg/dL)	200 (98 - 648)	211 (30 - 471)	0.57
Creatinine phosphokinase (30-223 U/L)	244 (30 - 2701)	300 (58 - 6000)	0.15
Albumin (3.5-5 g/dL)	3.2 (2.2 - 4.1)	**2.1 (1.6 - 3.3)**	**0.001**
D-dimer (0-0.24 µg/mL)	315 (134 - 7150)	**1666 (414 - 9567)**	**0.01**
Ferritin (11-307 ng/mL)	876.5 (116 - 2291)	827 (201 - 15000)	0.59
Fibrinogen (1.9-5.13 µg/mL)	4.6 (3.2 - 7.10)	**5.1 (4 - 7.8)**	**0.02**
Ca^{2+} (8.6-10.3 mg/dL)	7.9 (6.7 - 9.4)	7.4 (6 - 9)	0.06
Cl^{-} (98-107 pg/mL)	98.5 (90 - 109)	**102.5 (88 - 110)**	**0.03**
Na^{+} mmol/L (136-145)	132 (125 - 145)	136 (120 - 145)	0.22
K^{+} (3.5-5.1 mmol/L)	4 (3.1 - 5.2)	**5.3 (4.1 - 7.4)**	**0.003**
pro-B-type natriuretic peptide (15-125 pg/mL)	899 (110 - 13420)	1857 (340 - 25000)	0.06
Lactate (0.5-1.6 mmol/L)	2 (0.80 - 6.40)	1.7 (1.1 - 8)	0.51
Troponin (8.4-18.3 pg/mL)	37 (8.2 - 690)	**132 (8.6 - 27027)**	**0.001**
C reactive protein high sensitivity (1-3 mg/L)	192 (1.4 - 563)	296 (55 - 480)	0.30

parison it is between laboratories at the admission vs. death

Table 2. Characteristics of previous diseases and organ failure and complications during the evolution of infection by SARS-CoV-2

Characteristics and comorbidities prior to COVID-19												*Patients who progressed to KF*						
G	*Age*	*OW/O*	*Alc*	*Smoke*	*DL*	*MD*	*SAH*	*H*	*IHD*	*HF*	*AD*	*BCr*	*FCr*	*BBun*	*FBun*	*KF*	*Test*	*Symptoms and other complications*
M	*50*	+	-	-	-	-	-	-	-	-	-	*1.1*	*4.05*	*34*	*75.5*	+	+	*Fever, chills, and dyspnea (PE)*
M	*49*	+	-	-	-	-	-	-	-	-	-	*0.83*	*1.6*	*13.9*	*26.4*	-	+	*Fever, odynophagia, arthralgia, and myalgia*
M	*67*	+	+	+	-	+	+	-	-	-	-	*0.9*	*5.7*	*29*	*126.2*	+	+	*Fever, chills, arthralgia, asthenia, and dyspnea*
M	*62*	-	-	-	+	+	+	-	-	-	-	*2.12*	*1.87*	*31*	*61.1*	-	+	*Fever, cough, headache, and dyspnea*
M	*55*	-	+	-	-	-	-	-	+	-	-	*1.4*	*3.2*	*20.7*	*70.3*	+	+	*Chest pain, asthenia and adynamia (AMI)*
M	*62*	+	+	+	+	+	+	-	+	+	-	*1.59*	*7.15*	*50.5*	*92.9*	+	+	*Fever, chills, chest pain, cough, asthenia, adynamia and dyspnea (AMI)*
M	*59*	+	+	-	-	+	-	-	-	-	-	*0.92*	*0.79*	*12*	*33.7*	-	+	*Fever, somnolence, asthenia, adynamia, myalgia and dyspnea*
M	*74*	+	-	-	-	+	+	-	+	+	-	*1.68*	*3.1*	*46*	*256*	+	*PR*	*Dyspnea and cardiogenic shock*
M	*56*	+	-	+	-	-	-	-	-	-	-	*1.04*	*4.05*	*16.3*	*67.2*	+	-	*Fever, odynophagia, rhinorrhea, asthenia, adynamia, myalgia and dyspnea*
M	*50*	+	-	-	+	+	-	-	-	-	-	*1.3*	*4.9*	*55.4*	*145.1*	+	*PR*	*Fever, odynophagia, cough, and dyspnea*
M	*66*	+	-	+	-	+	-	-	-	-	-	*1.08*	*2.98*	*28.2*	*58.2*	+	+	*Fever, somnolence, asthenia, adynamia, dyspnea and septic shock*
M	*57*	+	+	-	-	-	-	-	-	-	-	*0.9*	*1.06*	*16*	*19*	-	+	*Fever, cough, and dyspnea*
F	*58*	-	-	-	-	+	-	-	-	-	-	*0.4*	*4.13*	*12*	*96.9*	+	+	*Fever, cough, headache, asthenia, arthralgia,*

																	myalgia diarrhea, dyspnea
F	*47*	+	-	-	-	-	-	-	-	-	+	*2.1*	*2.5*	*41.2*	*211*	+	+	*Fever, run nose, cough, arthralgia, myalgia, dysuria, and dyspnea*
F	*67*	-	-	-	-	+	+	+	+	-	-	*1.9*	*2.5*	*33*	*123*	+	+	*Cough and Dyspnea*

tions: G = Gender, M = male, F = Female, OW/O = overweight/Obesity, DL = dyslipidemia, MD = diabetes Mellitu arterial hypertension, H = hypothyroidism, IHD = ischemic heart disease, HF = heart failure, AD = autoimmune seline creatinine, FCr = final creatinine, BBun = baseline Blood urea nitrogen, FBun = Final Blood urea nitrogen, ilure, S = Suspect, PR = pending result, PE= pulmonary embolism, AMI = acute myocardial infarction. Abbreviat ıspartate aminotransferase, GOT = glutamic oxaloacetic transaminase, AAT = alanine aminotransferase, GPT = pyruvic transaminase. The informed consent for the publication of the data was obtained from participants/legal (s)/legally authorized representative/next of kin (for dead patients).

Figures

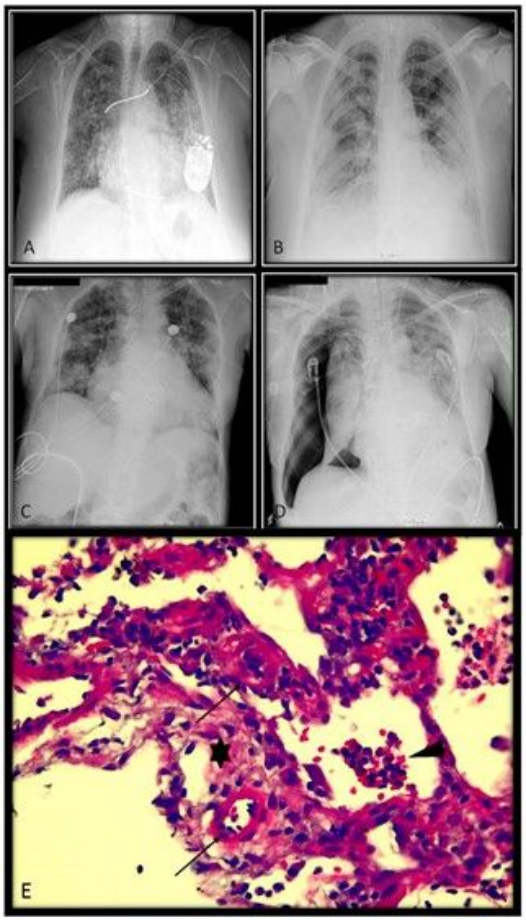

Figure 1

Representatives X-ray plates and photomicrograph of lung tissue from a COVID-19 patient observed at 40x. Panel A corresponds to a 58-year-old female COVID-19 patient with bilateral hilar opacities predominantly on the left side and cardiomegaly. The presence of a defibrillator with the distal end projected in RV can be observed. Panel B corresponds to a 67-year-old female patient with diffuse opacities predominantly in the left perihilar region. An endotracheal tube in proper position can be observed,

and the panel C and D correspond to a 56-year-old male patient. The studies were separated by 7 days of evolution. In the initial image (C), perihilar opacities with predominance on the right side and on the posterior radiography are observed while in panel D a right pneumothorax and increased radiopacities on the left side can be seen. These alterations were related with the lung histopathological changes in the panel E, where the changes of pneumonitis are observed. There is increased thickness of the alveolar walls, capillary congestion, and hyperplasia of pneumocytes indicated by arrowhead with the presence of moderate inflammatory infiltrate of polymorphonuclear leukocytes and alveolar macrophages indicated by arrows. There is also presence of moderate inflammatory infiltrate of polymorphonuclear leukocytes and alveolar macrophages. Histological sections were made and stained by H-E and observed at 40x.

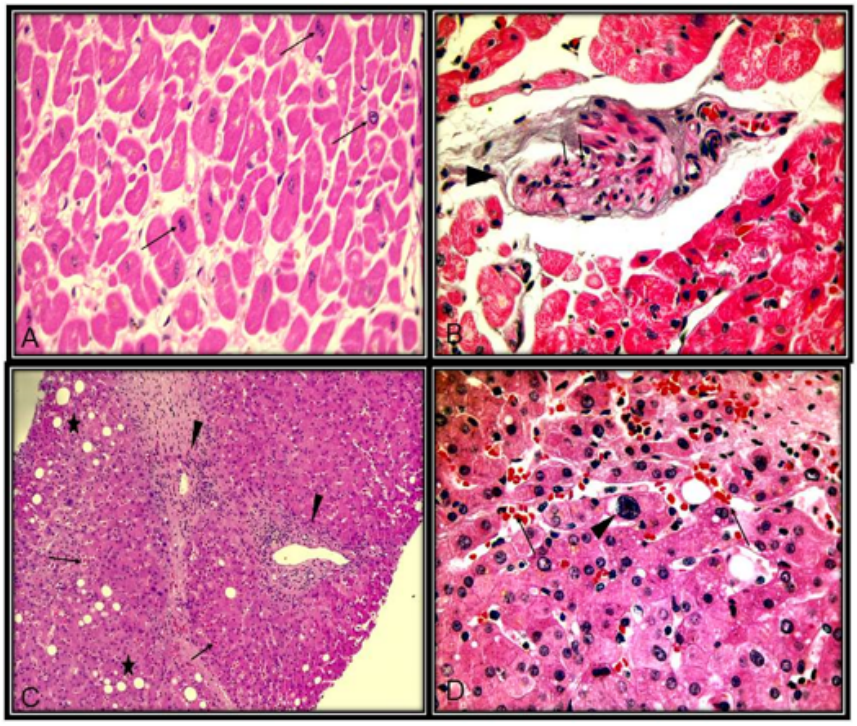

Figure 2

Representative photomicrographs of heart and liver tissue from a COVID-19 patient. Panel A corresponds to cardiac changes in a control patient. Mild changes of cardiac hypertrophy with variability in the size and shape of the nuclei (arrow), some with hyperchromatism. This sample was taken from a 60-year-old female patient with hepatocarcinoma, pulmonary micro-metastases and symptoms of pulmonary hypertension, without COVID-19 (10x). In comparison, panel B corresponds to representative photomicrograph of heart tissue from a COVID-19 patient. Close-up of the vessel (Arrowhead) shows hyperplasia of the wall with significant decrease in lumen and inflammatory infiltrate of lymphocytes indicated by arrows. Cardiomyocytes show degenerative vacuolization and the inflammatory cells are not observed (40x). Patients with underlying cardiovascular diseases are at a higher risk of becoming infected with coronavirus, and the course of the disease is more severe than in patients without heart disease. Due to these clinical conditions, the changes of chronic diseases overlap with those of the SARS-CoV virus, as shown in the panel B. The panel C (10x) and D (40x) corresponds to representative photomicrographs of liver tissue from a COVID-19 patient. The preserved morphology is observed; however, there is an increase in the inflammatory infiltrate by lymphocytes in the portal spaces which is indicated by arrowhead. There is also an increase in fibro connective tissue, steatosis indicated by star, and congestion in the sinusoids indicated by arrows as shown in the panel C). The arrowhead shows enlarged hepatocyte with finely granular cytoplasm. The cytopathic changes are apparent; with an increase in the size of the nucleus which is at least four times bigger than the ones that surround it. Congestion in the sinusoids is indicated by arrows. In the liver, the columnar epithelial cells of the bile ducts do not show histological alterations. However, the columnar epithelial cells of the bile ducts do not show histological alterations as shown in the Panel D). Histological sections were made with H-E stain.

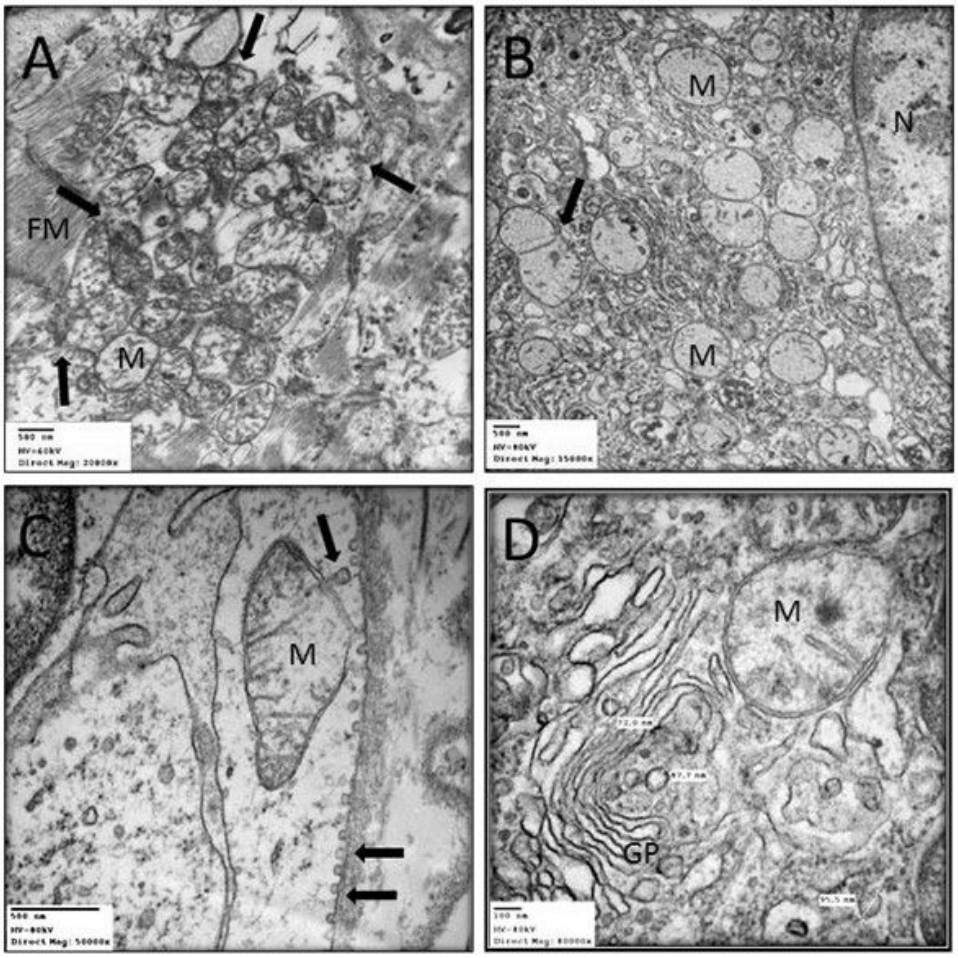

Figure 3

Representative electron micrograph of different organs from COVID-19 patients at different magnifications. Panels A: heart (cardiomyocyte), B: liver (hepatocyte), C and B lung tissue (pulmonary hilum cell). Panel A: Interfibrillary mitochondria are shown with loss of continuity of the outer membrane. There are areas of mitochondrial fusion with loss of inner ridges and electro dense areas in the fusion, but most are electro-lucid due to the loss of the matrix. Magnification at 20000x. Panel B: as in the heart, mitochondrial changes are maintained where mitochondrial fusion is shown again. Magnification at 15000x. Panel C: Lung macrophage where viral particles are observed in transition from the outer to the inner membrane; and a mitochondrion with loss of internal ridges and rupture of the external membrane where we can see a viral particle entering or leaving it. Magnification at 50000x. Panel D: Type II pneumocyte, where the Golgi apparatus and mitochondria with loss of internal ridges and the presence of viral particles are observed, which were measured. Magnification at 80000x. The viral particles were found ranging in size from 72 to 95.5 nm. Abbreviations: CF = cardiac fibers, FZ = fusion zone, GP = Golgi apparatus, N = nucleus, M = mitochondria, VP = viral particles.

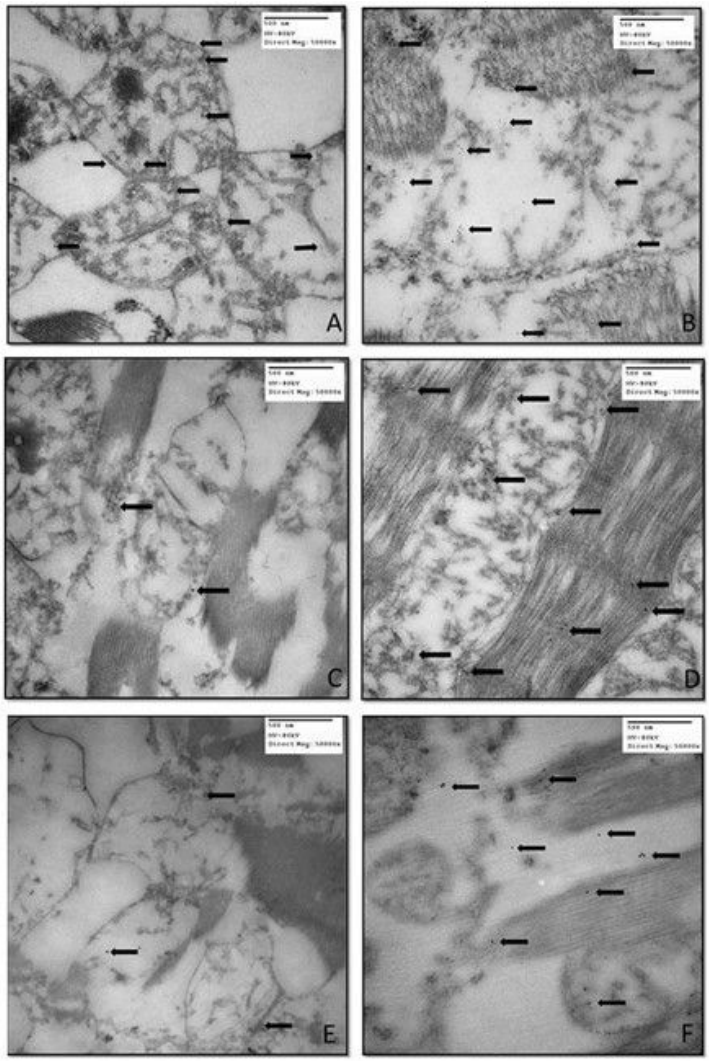

Figure 4

Representative electron micrograph of heart tissue from: A, C and E = control subject, B, D and F = COVID-19 patient at 50000x. In panels A and B the arrows indicate the presence of the immune colloidal 10nm gold marker COX II in the sample from a COVID-19 patient. Membrane breaking are observed, and loss of the ridges of the inner membrane of the mitochondria. The subunit marker was present both on ridges and on the muscle fibers. This was not observed in the sample from the control. In panels C and D the arrows indicate the presence of the subunit of the immune colloidal 15nm gold marker for COX IV. There is a mitochondrion between cardiac muscle fibers in which the subunit marker was present both on ridges and the muscle fibers. In comparison, these changes were not observed in the control subject. In Panels E and F the arrows indicate the presence of the immune colloidal 15nm gold marker for MnSOD, which is an antioxidant enzyme. Mitochondria are present between cardiac muscle fibers. The electrodense zone marker was present both on ridges and on the muscle fibers. In comparison, in the control subject, the electrodense zones of the marker were only present inside the mitochondrial matrix.

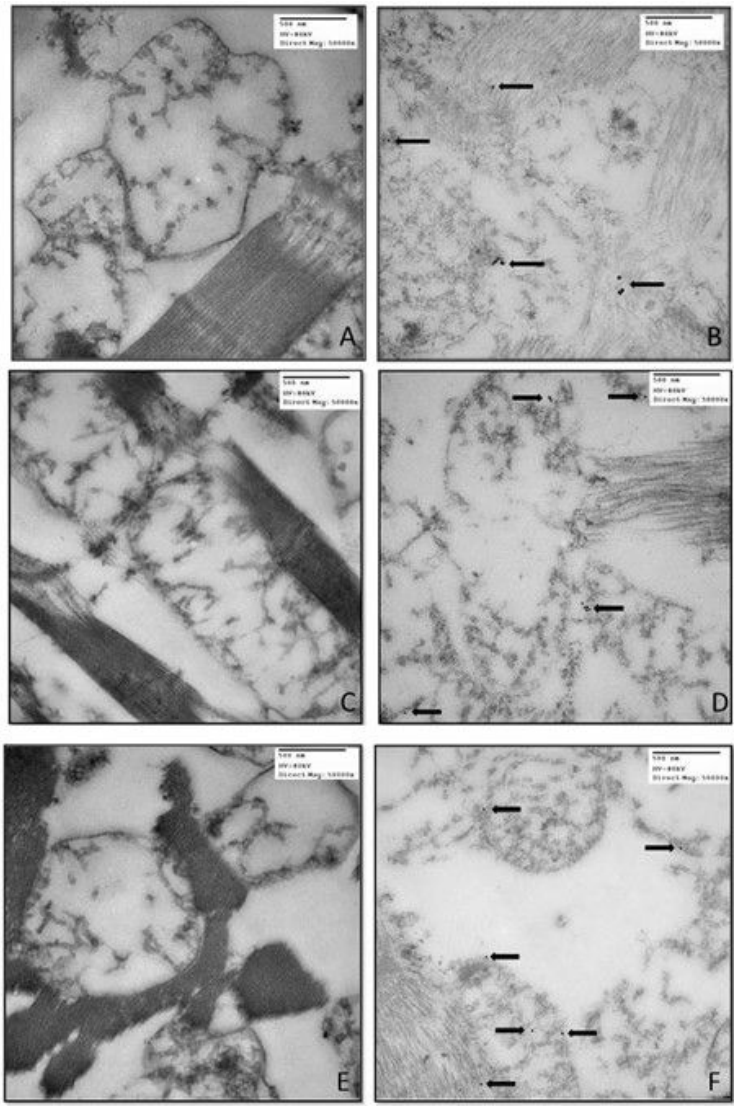

Figure 5

Representative electron micrographs of heart tissue (cardiomyocytes) from: Panels A, C and D control subject, Panels B, E and F COVID-19 patient at 50000x. In panels A and B the arrows indicate the presence of the immune colloidal 25 nm gold marker for nitrotyrosine protein. There are mitochondria between cardiac muscle fibers and the electrodense zone marker was present both on ridges and the muscle fibers. In comparison these changes were not observed in the control subject. . In panels C and D the arrows indicate the presence of the immune colloidal 15 nm gold marker for caspase 9. The electrodense zone marker was present only in the mitochondrias of the COVID-19 patients. The electrodense zones were not present in the control subject. In panels E and F the arrows indicate the presence of the immune colloidal 15nm gold marker for Bcl-2 marker. Mitochondria are present between in cardiac muscle fibers and the electrodense zones marker was present only in the mitochondrias from the COVID-19 patient. In the control subject, the electrodense zones were not present.

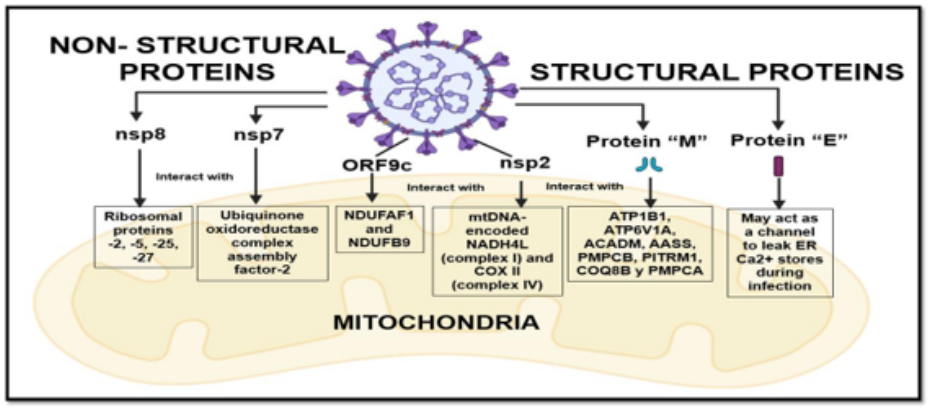

Figure 6

Summary of the possible interactions of the different structural and non-structural proteins of the SARS-CoV-2 with the mitochondria. The RNA genome of this virus codes for structural and non-structural proteins. Four groups of proteins characterize the SARS-CoV-2. 1) viral envelope proteins (E) that include the spike structural glycoprotein (S) with prominent projections on the surface, the nucleocapsid (N) protein and the matrix protein (M), 2) proteases nsp1-nsp16, that participate as inhibitors of multiple steps of translation initiation (Lu et al., 2016), 3) a RNA-dependent RNA polymerase (RdRp) which is a non-structural protein and 4) a set of 4 or more 3' conterminal sub-genomic mRNAs replicase whose genes are composed of two overlapping open reading frames (Lu et al., 2016). The M protein determines the shape of the viral particle and binds to the nucleocapsid (Ibrahim et al., 2020). The E protein participates in viral particle release while the N protein helps in the RNA binding to the host transcription complex participating in viral replication. The N protein interacts with the viral RNA to form the nucleocapsid and is responsible for distributing the viral ribonucleoprotein complex for replication; this protein may also promote the degradation of the MAVS, which acts as an adapter for transcription and production of IFNs being the most potent antiviral cytokine. The viral nsp are proteins that participate in synthesis or processing of viral RNA, or in virus-host interactions aiming to create an optimal environment for the replication of the coronavirus. The nsp3, nsp4, and nsp6 proteins of the coronaviruses have been implicated in the process of the viral membrane formation. The viral protein nsp8 may interact with mitochondrial ribosomal protein S-2, -5, -25, -27 and the viral protein nsp7 may to interact with the mitochondrial protein ubiquinone oxidoreductase complex assembly factor-2. The ORF9c can interact with the mitochondrial protein NADH dehydrogenase ubiquinone 1 α sub-complex assembly factor-1 (NDUFAF1) and NADH dehydrogenase ubiquinone 1 β sub-complex subunit-9 (NDUFB9). The NDUFB9 is an essential subunit of complex I and NDUFAF1 and -2 are critical players involved in the assembly of complex I. Moreover, the viral protein M can interact with ATP1B1, ATP6V1A, ACADM, AASS, PMPCB, PITRM1, COQ8B, and PMPCA, which are part of the critical metabolic pathways carried out in the mitochondria. This protein may also interfere with the posttranscriptional machinery of the host by blocking the nuclear transport of spliced mRNAs and small nuclear RNAs and by slowing the nuclear transport of many other molecules. Furthermore, the viral protein nsp2 of the SARS-CoV-1 can interact with the prohibiting protein PHB and nsp10 to interact with mitDNA-encoded NADH4L (complex I) and COX II (complex IV). Besides, E protein of the SARS-CoV-1 may act as a channel to leak ER Ca2+ stores during infection. Regarding other viruses, viral protein nsp4 of the rotavirus can induce Ca2+ mobilization in infected human epithelial cells. Maintenance of mitochondrial/cellular Ca2+ homeostasis is vital for various cellular functions. Abbreviations: NDUFAF1 = NADH dehydrogenase ubiquinone 1 α sub-complex assembly factor-1, NDUFB9 = NADH dehydrogenase ubiquinone 1 β sub-complex subunit-9.

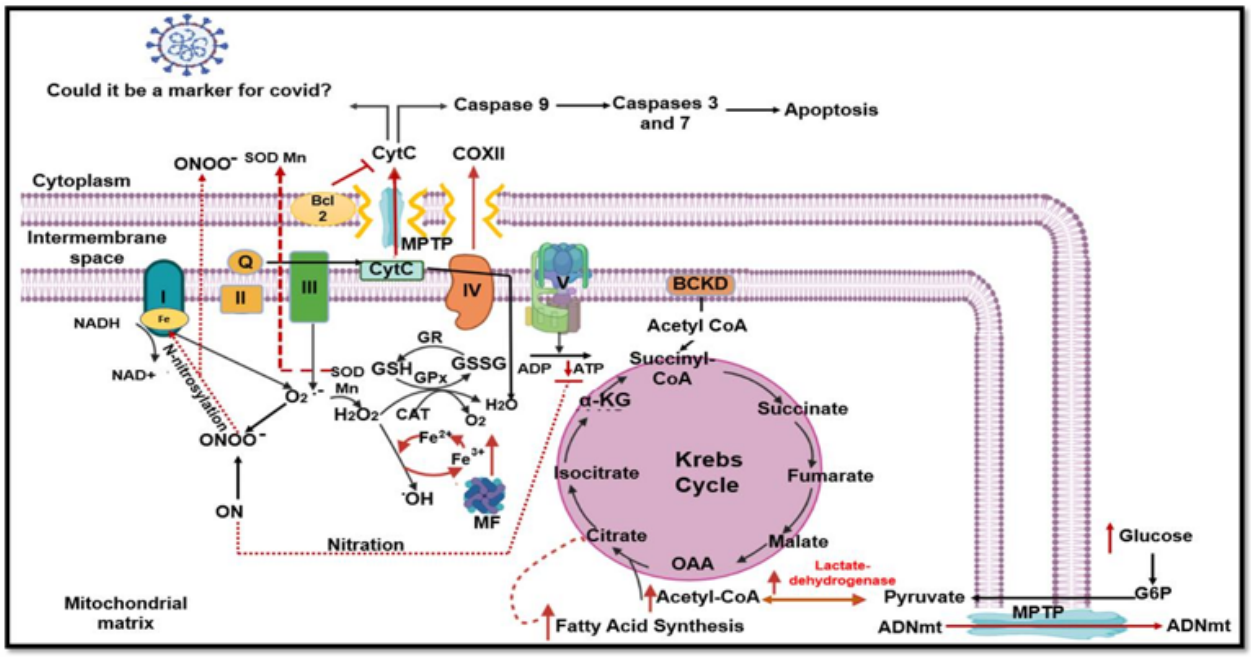

Figure 7

Summary of mitochondrial alterations and possible damage caused by SARS-CoV-2. Viral envelope proteins E may act as channels to leak Ca2+ stores from the endoplasmic reticulum and other organelles during infection. The N viral protein mediates an ubiquitination process that degrades MAVS. The viral M protein interacts with critical mitochondrial metabolic pathways. Mitochondrial function is also regulated by the serine protease TMPRSS2 via the estrogen-related α-receptor, which transcriptionally regulates energy homeostasis. This protease is a key enzyme for the entry of SARS-CoV-2 into the host cells since it binds to the ECA2 receptor when it is linked to the virus through its S protein (Petersen et al., 2001). Abbreviations: CytC = cytochrome C, ONOO− = peroxynitrite, MPTP = mitochondrial permeability transition pore, SOD = superoxide dismutase, CAT = catalase, GPx = glutathione peroxidase, GR = glutathione reductase, GSH = glutathione, GSSG = oxidized glutathione, ON = oxide nitric, OH = hydroxyl radical, BCKD = branched chain keto acid dehydrogenase, α-KG = indicates α-ketoglutarate, OAA = oxaloacetate, G6P = glucose-6-phosphate, MF = mitochondrial ferritin.